Informatics in Medicine Unlocked 34 (2022) 101105

Contents lists available at ScienceDirect

Informatics in Medicine Unlocked

journal homepage: www.elsevier.com/locate/imu

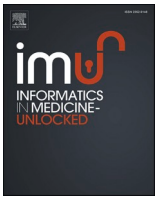

Artificial intelligent investigations for the dynamics of the bone transformation mathematical model

Watcharaporn Cholamjiak [a], Zulqurnain Sabir [b], Muhammad Asif Zahoor Raja [c], Manuel Sánchez-Chero [d,e], Dulio Oseda Gago [f], José Antonio Sánchez-Chero [g], María-Verónica Seminario-Morales [g], Marco Antonio Oseda Gago [h], Cesar Augusto Agurto Cherre [i], Gilder Cieza Altamirano [j], Mohamed R. Ali [k,*]

[a] School of Science, University of Phayao, Phayao, 56000, Thailand
[b] Department of Mathematics, Hazara University, Mansehra, 21120, Pakistan
[c] Future Technology Research Center, National Yunlin University of Science and Technology, 123 University Road, Section 3, Douliou, Yunlin, 64002, Taiwan, ROC
[d] Universidad Nacional de Frontera, Sullana, Peru
[e] Facultad de Ingeniería de Industrias Alimentarias y Biotecnología, Peru
[f] Universidad Nacional Mayor de San Marcos, Lima, Peru
[g] Facultad de Ciencias Económicas y Ambientales, Universidad Nacional de Frontera, Sullana, Peru
[h] Universidad Nacional Ciro Alegría, Peru
[i] Universidad Nacional de Ucayali, Ucayali, Perú, Facultad de Ingeniería de Sistemas e Ingeniería Civil, Peru
[j] Universidad Nacional Autónoma de Chota, Fizmako Research Group, Cajamarca, Peru
[k] Faculty of Engineering and Technology, Future University, Cairo, Egypt

ARTICLE INFO

Keywords:
Fractional order
Bone transformation
Myeloma disease
Scale conjugate gradient procedures
Artificial neural networks
Cell dynamics

ABSTRACT

In this study, the stochastic numerical solutions of the fractional myeloma bone disease system (FMBDS) have been presented. The fractional order investigation provides more accurate solutions of the FMBDS. The FMBDS is classified into three dynamics and the solution of each class is presented by using the artificial neural network enhanced by the scale conjugate gradient procedures (ANN-SCGPs). Three different fractional order performances have been used to present the solutions of the FMBDS by applying the ANN-SCGPs. The statics is chosen as 11%, 12% and 77% for training, testing and verification. Twelve number of hidden neurons with input and output layers have been proposed for the FMBDS. The comparison of proposed and reference solutions is performed that shows the accuracy of the ANN-SCGPs. The consistency, validity, precision, and capability of the ANN-SCGPs can be judged based on the state transitions values, regression actions, correlation behaviors, error histograms, and mean square error data.

1. Introduction

Remodeling is the process through which bone is continuously replaced throughout the skeleton. The bone formation procedure occupies 5–25% of the bone's surface and heterogeneous, with asynchronous cycles at numerous places [1]. Every component of the skeleton is periodically modified throughout time in this way. The process of bone remodeling has been mathematically modeled in numerous ways. Models of Michaelis-Menten-like regulatory mechanisms on bone resorption are among these approaches to consider how bone growth is induced by biomechanical stress [2–6]. Other simulation projects have looked at the signaling pathways in the osteoblasts and osteoclasts intricated in the remodeling of bone or taken into consideration of both activities based on the microenvironment called as elementary multicellular unit [7–11].

A hematological cancer called multiple myeloma is brought by using the clonal proliferation of malignant plasma cells in bone marrow. One of the clinical manifestations of myeloma is the onset of an osteolytic

* Corresponding author.
E-mail addresses: watcharaporn.ch@up.ac.th (W. Cholamjiak), zulqurnain_maths@hu.edu.pk (Z. Sabir), rajamaz@yuntech.edu.tw (M.A.Z. Raja), msanchezch@unf.edu.pe (M. Sánchez-Chero), dosedag@unmsm.edu.pe (D.O. Gago), jsanchez@unf.edu.pe (J.A. Sánchez-Chero), mseminario@unf.edu.pe (M.-V. Seminario-Morales), profesional.dpbs@unca.edu.pe (M.A.O. Gago), cesar_agurto@unu.edu.pe (C.A.A. Cherre), gciezaa@unach.edu.pe (G.C. Altamirano), Mohamed.Reda@fue.edu.eg (M.R. Ali).

https://doi.org/10.1016/j.imu.2022.101105
Received 4 September 2022; Received in revised form 6 October 2022; Accepted 6 October 2022
Available online 12 October 2022

Table 1
Description of the parameter for the FMBDS.

Parameter	Descriptions
$g_{BB}, g_{BC}, g_{CC}, g_{CB}$	Autocrine regulator
β_B, β_C	Apoptosis rate
α_C, α_B	Activation rate
$r_{BB}, r_{BC}, r_{CC}, r_{CB}$	Autocrine of tumorous and paracrine instruction
L_T	Metastases bone magnitude
γ_T	Growth metastases rate
l_1, l_2, l_3	Initial conditions

bone disease that progresses and is destructive, accompanied by severe hypercalcemia, pathological fractures, bone pain, osteoporosis, and compression of the backbone cord. For myeloma to grow/survive and osteolytic bone disease to develop, connections between bone marrow myeloma microenvironment cells are essential [12,13]. Because of vicious loop that forms between myeloma cells and the bone marrow microenvironment, myeloma bone illness has a greater propensity for destruction.

Resorption and production become uncoupled in the aberrant bone remodeling, which arises in various myeloma patients, which leads to an increase in bone resorption and a decrease in bone creation. In close proximity to regions of active bone resorption, myeloma cells have been extensively documented for their capacity to induce osteoclast development and production [14–16]. In the early stages of myeloma, bone production is actually boosted, as per histological investigations. This is assumed to be an effort to make up the rise in osteoclastic resorption. Bone formation, however, dramatically declines as the condition worsens [17,18]. Studies showing that multiple myeloma patients have lower levels of bone formation markers with their support [19,20]. Multiple myeloma is still an incurable cancer despite many important improvements in our understanding of its biology, and the devastating osteolytic bone disease is a primary source of morbidity in individuals with multiple myeloma.

The bone remodeling based on the tumor growth shows that how tumor effects paracrine and autocrine signaling the osteoblast and osteoclast using the cell populations. The feedback from osteoblasts and osteoclasts that controls each cell type's development is known as autocrine signaling. Paracrine signaling is a representation of the factors released by osteoclasts that regulate osteoblast formation, and the other way around. The underlying system based on the bone remodeling is used in the nonappearance of tumor [21–24]. This dynamical system has no explicit spatial dimensions, but it does have a dependent variable that tracks bone mass over time. If the bone mass system is applied as a local trabecular mass beneath a surface point of the bone, then dimension based on one spatial is presented.

A mathematical system based on the fractional myeloma bone disease system (FMBDS) has been presented in this study. The fractional order derivatives have been used in various applications to find the accurate performances. The FMBDS is categorized into three classes and the solution of each category is presented by applying the artificial neural network along with the scale conjugate gradient procedures (ANN-SCGPs). The stochastic computing approaches based on the ANN-SCGPs have been used before to solve the mathematical FMBDS. Recently, the stochastic solvers had abundant applications in the food chain dynamical models [25–27], singular differential system [28–30], eye surgery differential models [31,32], smoking mathematical models [33,34], nonlinear biological Leptospirosis system [35,36] and nervous stomach models [37,38]. By keeping these applications into mind, the authors are interested to solve the mathematical form of the FMBDS stochastically. Few novel features of this study are presented as:

- A mathematical model based on FMBDS along with the effects of tumor is presented.
- The fractional order study is used to find more realistic solutions of the biological based nonlinear differential model.
- The computational stochastic procedures based on ANN-SCGPs have been implemented to solve the FMBDS.
- The solutions of three fractional order cases of the model have been accessible for the mathematical FMBDS.
- The correctness of the scheme is observed through the comparison performances of the proposed and reference Adam solutions.
- The accuracy of the scheme is observed in term of state transitions (STs) values, regression actions, correlation behaviors and error histograms (EHs) for solving the mathematical nonlinear FMBDS.

The remaining sections of the paper are provided as: Section 2 represents the design of the FMBDS, Section 3 shows the methodology of the scheme, Section 4 presents the numerical solutions of the FMBDS and final Section indicates the concluding remarks.

2. Mathematical model of the FMBDS

In this section, the mathematical form of the FMBDS is presented. The presence of myeloma disturbs the consistent cycles of normal bone system. The mathematical form of the integer order system is given as [39]:

$$\begin{cases} \dfrac{dC(\theta)}{d\theta} = -\beta_C C(\theta) + \alpha_C B(\theta)^{g_{BC}\left(r_{BC}\frac{T(\theta)}{L_T}+1\right)} C(\theta)^{g_{cc}\left(r_{CC}\frac{T(\theta)}{L_T}+1\right)}, C_0 = l_1, \\ \dfrac{dB(\theta)}{d\theta} = -\beta_B B(\theta) + \alpha_B B(\theta)^{\left(-r_{BB}\frac{T(\theta)}{L_T}+g_{BB}\right)} C(\theta)^{\left(\frac{g_{CB}}{r_{CB}\frac{T(\theta)}{L_T}+1}\right)}, B_0 = l_2, \\ \dfrac{dT(\theta)}{d\theta} = \gamma_T \log\left(\dfrac{L_T}{T(\theta)}\right) T(\theta), T_0 = l_3. \end{cases} \tag{1}$$

Where $C(\theta)$ and $B(\theta)$ represent the densities of the osteoclasts and osteoblasts, while $T(\theta)$ presents the tumor cells density at time θ. The description of each parameter that is used in equation (1) is presented in Table 1 as:

The numerical performances of the mathematical FMBDS have been acheived in these investigations by applying the procedures of artificial intelligence (AI) along with the stochastic computing framework based on the ANN-SCGPs. Recently, the stochstic procedure have been implemented in various disease model based applications, like as novel discrete coronavirus fractional model [40], fractional order dynamical nonlinear susceptible infected and quarantine differential model [41], fractional order novel food supply system [42], immune-chemotherapeutic treatment for breast cancer [43], and SIDARTHE coronavirus differential pandemic model [44].

The mathematical FMBDS have been presented to analyse the performances based super slow evolution or superfast progressions by using the fractional derivatives as:

$$\begin{cases} \dfrac{d^{\upsilon}C(\theta)}{d\theta^{\upsilon}} = -\beta_C C(\theta) + \alpha_C B(\theta)^{g_{BC}\left(r_{BC}\frac{T(\theta)}{L_T}+1\right)} C(\theta)^{g_{cc}\left(r_{CC}\frac{T(\theta)}{L_T}+1\right)}, sC_0 = l_1, \\ \dfrac{d^{\upsilon}B(\theta)}{d\theta^{\upsilon}} = -\beta_B B(\theta) + \alpha_B B(\theta)^{\left(-r_{BB}\frac{T(\theta)}{L_T}+g_{BB}\right)} C(\theta)^{\left(\frac{g_{CB}}{r_{CB}\frac{T(\theta)}{L_T}+1}\right)}, B_0 = l_2, \\ \dfrac{d^{\upsilon}T(\theta)}{d\theta^{\upsilon}} = \gamma_T \log\left(\dfrac{L_T}{T(\theta)}\right) T(\theta), T_0 = l_3. \end{cases} \tag{2}$$

where υ indicates the fractional order Caputo derivatives for solve the FMBDS by applying the ANN-SCGPs. The values of the fractional order υ are taken between 0 and 1.

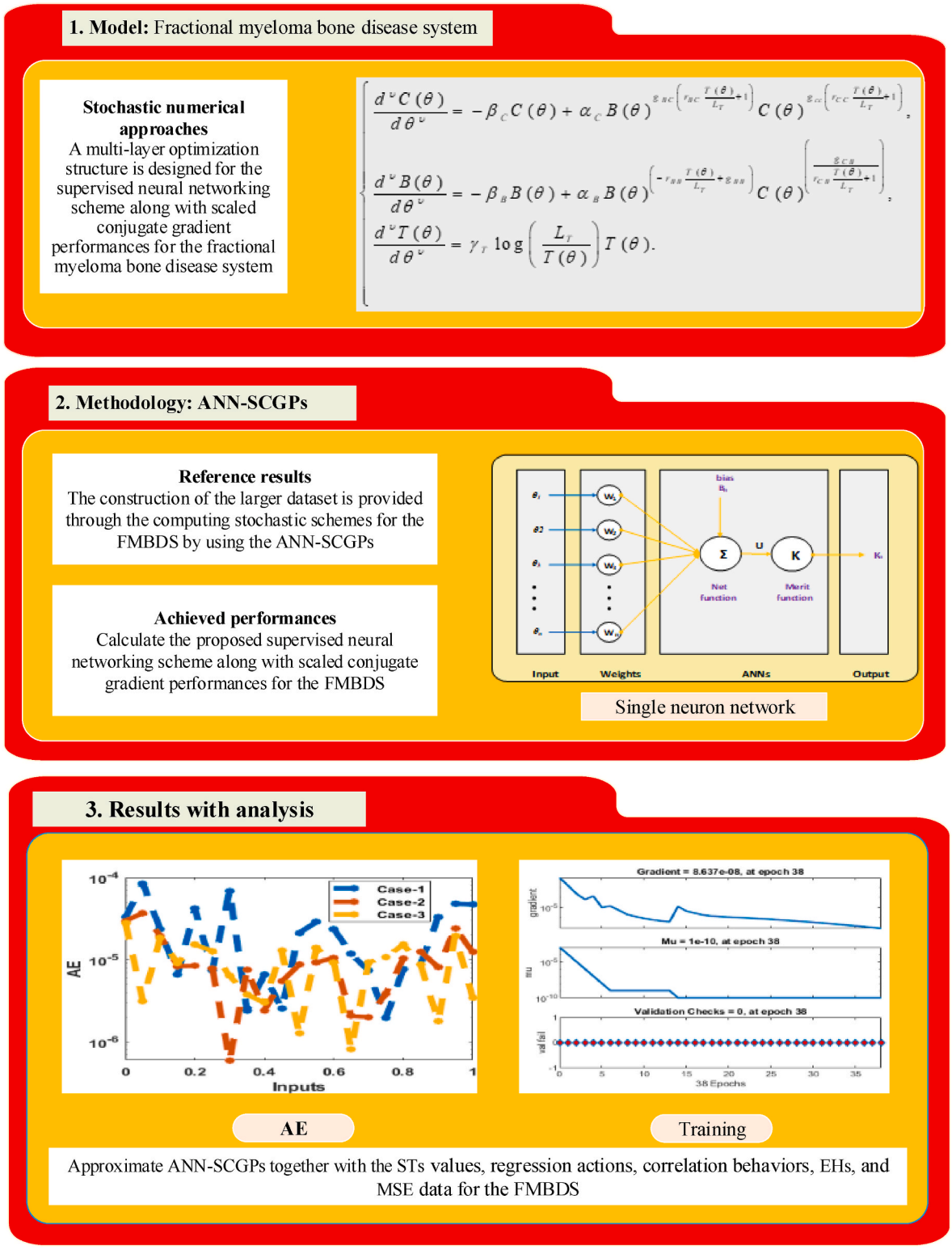

Fig. 1. Workflow illustrations using the using the ANN-SCGPs for the FMBDS.

Table 2
Implementation performances using the ANN-SCGPs.

Index	Settings
Authentication data	77%
Test data	12%
Fitness (MSE)	0
Hidden/input/output layers	Single
Reduction in mu values	0.4
Selection of data	Random
Maximum performances of mu	10^{9}
Maximum learning Epochs	600
Dataset	Adam's method
Adaptive values of the parameter	0.002
Train data	11%
Increasing factor of mu	09
Hidden neurons	12
Verification count fails	07
Minimum gradient measures	10^{-07}
Adam's method and terminating values	Default

3. Procedure based ANN-SCGPs

The structure of the ANNs-SCGPs for FMBDS has been presented by using the execution performances of the scheme along with the significance operator measures. Fig. 1 represents the stochastic multi-layer optimization procedures using the ANN-SCGPs. The statics is selected as 11%, 12% and 77% for training, testing and verification. Twelve hidden numbers of neurons with input and output layers have been used in these investigations to solve the FMBDS.

The parameter implementation procedures by applying the ANN-SCGPs are shown in Table 2.

4. Results and discussions

The current section shows three distinct values of the fractional order derivative of the FMBDS haven been taken. The solutions of these three variations by using the ANN-SCGPs have been provided to solve the FMBDS. The mathematical form of the FMBDS is given as:

Case 1: Consider the values $\upsilon = 0.5$, $L_T = 0.14$, $\gamma_T = 0.22$, $\beta_B = 0.25$, $\alpha_B = 0.22$, $\beta_C = 0.1$, $\alpha_C = 0.12$, $r_{CC} = 0.18$, $r_{BB} = 0.1$, $r_{BC} = 0.2$, $g_{BB} = 0.09$, $r_{CB} = 0.19$, $g_{CC} = 0.16$, $g_{CB} = 0.17$, $g_{BC} = 0.15$, $l_1 = 0.1$, $l_2 = 0.2$ and $l_3 = 0.3$ in equation (2).
Case 2: Consider the values $\upsilon = 0.6$, $L_T = 0.14$, $\gamma_T = 0.22$, $\beta_B = 0.25$, $\alpha_B = 0.22$, $\beta_C = 0.1$, $\alpha_C = 0.12$, $r_{CC} = 0.18$, $r_{BB} = 0.1$, $r_{BC} = 0.2$, $g_{BB} = 0.09$, $r_{CB} = 0.19$, $g_{CC} = 0.16$, $g_{CB} = 0.17$, $g_{BC} = 0.15$, $l_1 = 0.1$, $l_2 = 0.2$ and $l_3 = 0.3$ in equation (2).
Case 3: Consider the values $\upsilon = 0.7$, $L_T = 0.14$, $\gamma_T = 0.22$, $\beta_B = 0.25$, $\alpha_B = 0.22$, $\beta_C = 0.1$, $\alpha_C = 0.12$, $r_{CC} = 0.18$, $r_{BB} = 0.1$, $r_{BC} = 0.2$, $g_{BB} = 0.09$, $r_{CB} = 0.19$, $g_{CC} = 0.16$, $g_{CB} = 0.17$, $g_{BC} = 0.15$, $l_1 = 0.1$, $l_2 = 0.2$ and $l_3 = 0.3$ in equation (2).

The performances to find the numerical solutions based on the ANN-SCGPs for the FMBDS haven presented. The statics is chosen as 11%, 12% and 77% for training, testing and verification. Twelve number of hidden neurons with input and output layers have been proposed in this study for FMBDS. The input/hidden/output hidden layers structure is presented in Fig. 2.

Figs. 3–5 indicates the ANN-SCGPs procedure for solving the mathematical form of the FMBDS. Fig. 3 illustrates the values of the MSE and STs for FMBDS and Fig. 4 shows the perfect EHs, curves, validations, and STs for the mathematical form of the FMBDS. The optimal values of FMBDS have been presented at iterations 38, 63 and 40 that are 2.34645×10^{-09}, 2.56690×10^{-10}, and 4.59596×10^{-10}. The gradient measures for case 1 to 3 are 8.64×1930^{-08}, 9.77×10^{-08}, and $9. \times 10^{-08}$. Fig. 4 indicates the computational performances along with the values of the EHs for the mathematical form of FMBDS based on ANN-SCGPs. The achieved and reference solution performances have been presented to access the exactness of the approach. The solutions of the FMBDS based on the ANN-SCGPs based on the authentication, training and testing have been also drawn. Fig. 4 represents the values of EHs that are 3.85×10^{-06}, 7.13×10^{-06}, and -7.3×10^{-07} for case 1 to 3. Fig. 5 represents the correlation measures based on ANN-SCGPs for the FMBDS. The correlation performances using the ANN-SCGPs have been presented for the FMBDS. The accuracy of the ANN-SCGPs for the mathematical FMBDS has been presented based on the training, authentication and testing measures. Table 3 shows the MSE measures for the FMBDS using the verification, training, complexity, iterations and backpropagation.

Figs. 6 and 7 indicate the exactness of ANN-SCGPs for the FMBDS using the comparison of the solutions and the performances of the AE. The obtained numerical measures have been provided for the nonlinear mathematical FMBDS using the ANN-SCGPs. These overlapping of the results have been performed in Fig. 6. The AE values for the nonlinear mathematical FMBDS using the AI based procedures have been illustrated in Fig. 7. The AE for the $C(\theta)$ and have been calculated as 10^{-04} to 10^{-05} for 1st case, while the AE for rest of the cases found as 10^{-05} to 10^{-06}. The performances of the AE for $B(\theta)$ are calculated as 10^{-04} to 10^{-06} for each case of the mathematical FMBDS. The AE for $T(\theta)$ lie as 10^{-04} to 10^{-05} for case 1, while the AE for other two cases found as 10^{-05} to 10^{-06}. These optimal AE measures indicate the correctness of the ANN-SCGPs for the mathematical FMBDS.

5. Conclusion

The purpose of these investigations is to propose the stochastic performances of the fractional myeloma bone disease system to get more realistic solutions. The dynamics of the FMBDS is categorized into three classes and the solution of each class is presented by using the ANN-SCGPs. Some concluding remarks of this study are presented as:

- The stochastic numerical solutions have been presented first time to solve the mathematical FMBDS.
- Three different variations of the fractional order derivatives have been presented to present the numerical performances of FMBDS by applying the ANN-SCGPs.
- The selection of the data is performed as 11%, 12% and 77% for training, testing and verification.
- Twelve number of hidden neurons with output and input layer structure have been proposed to solve the FMBDS using the ANN-SCGPs.

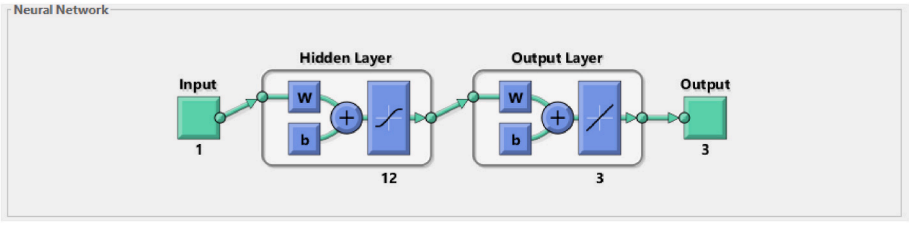

Fig. 2. Input/hidden/output layers structure using the ANN-SCGPs for FMBDS.

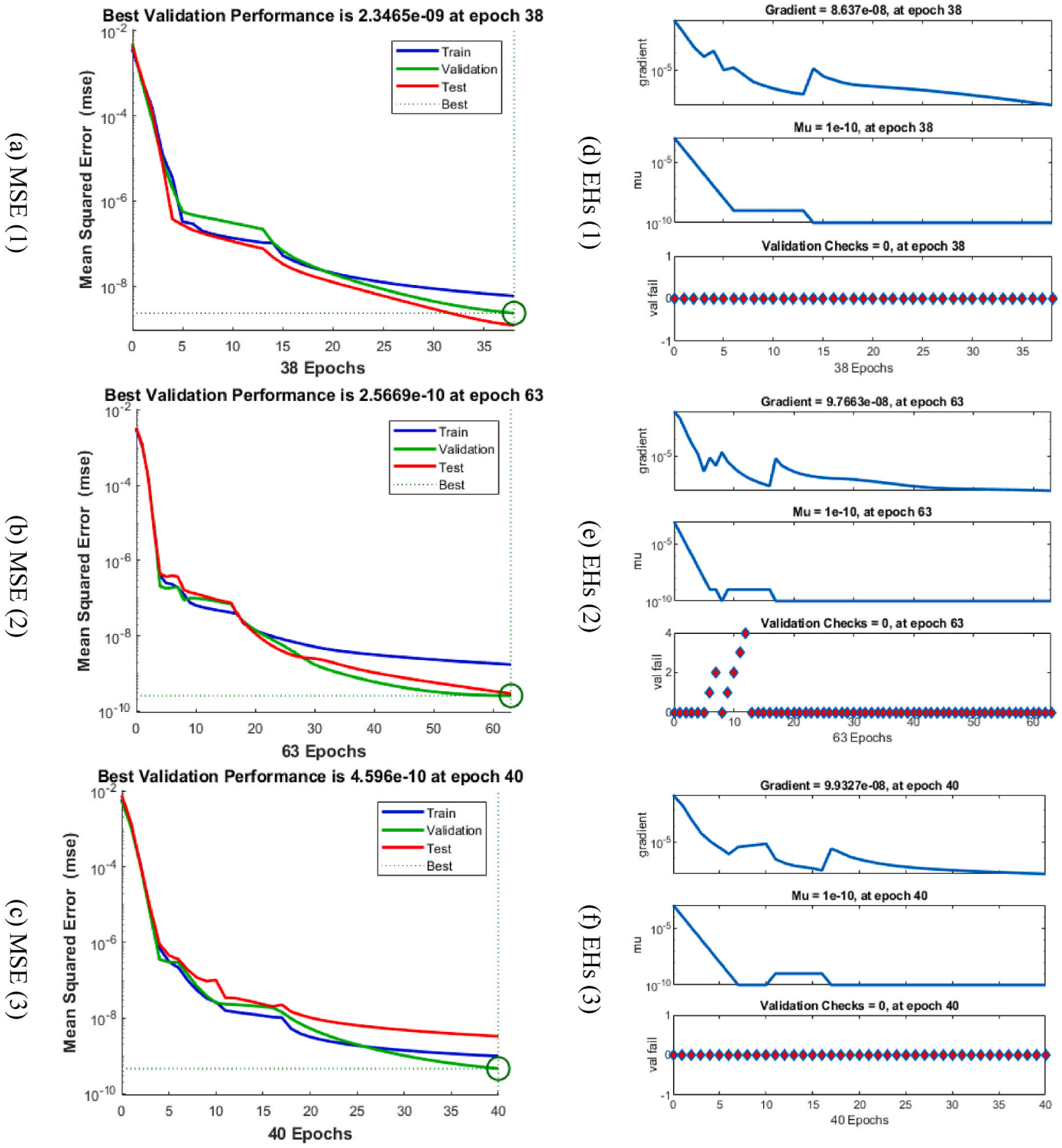

Fig. 3. The values of the MSE and STs for the FMBDS.

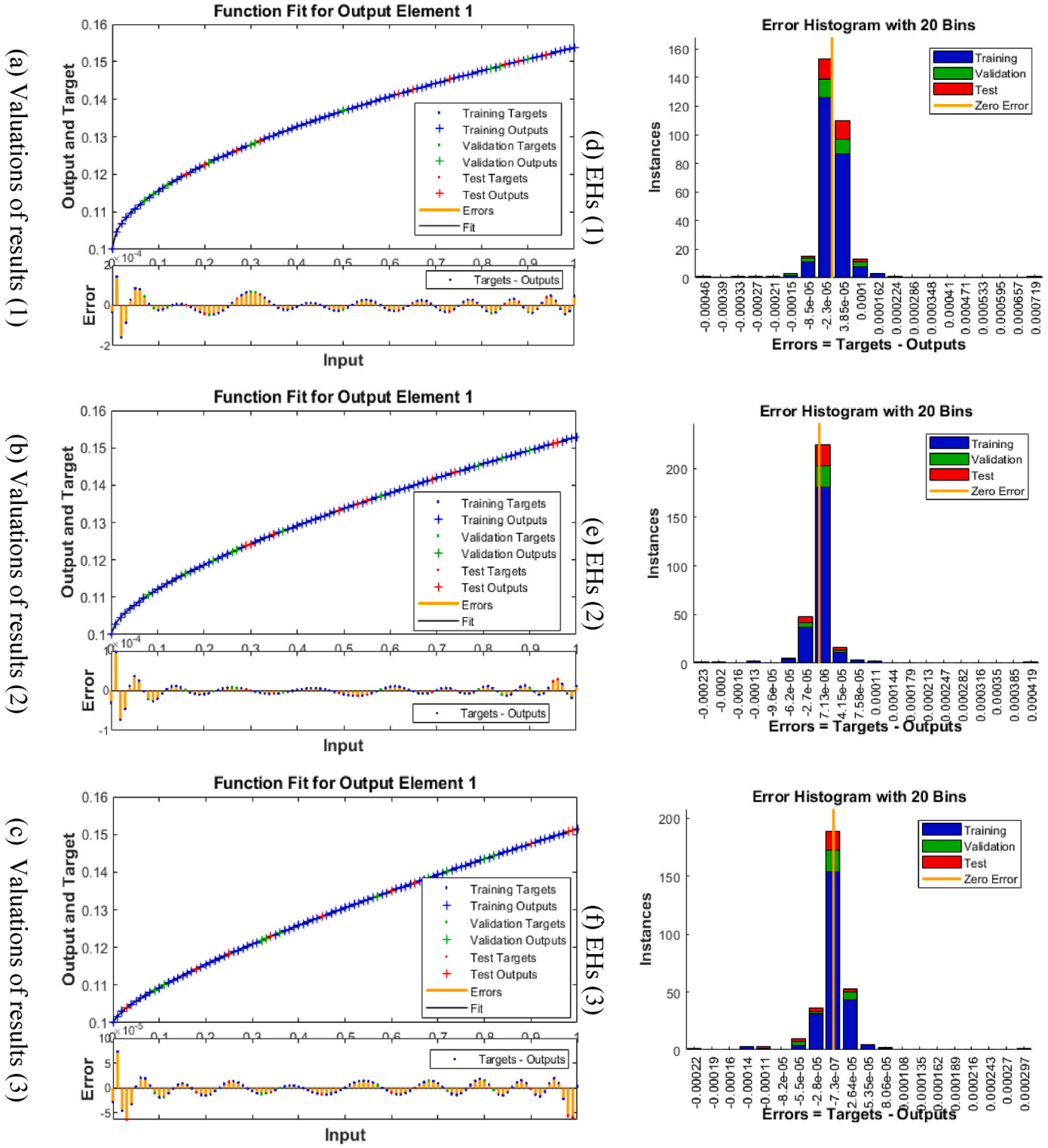

Fig. 4. Valuations of the results and EHs for the FMBDS.

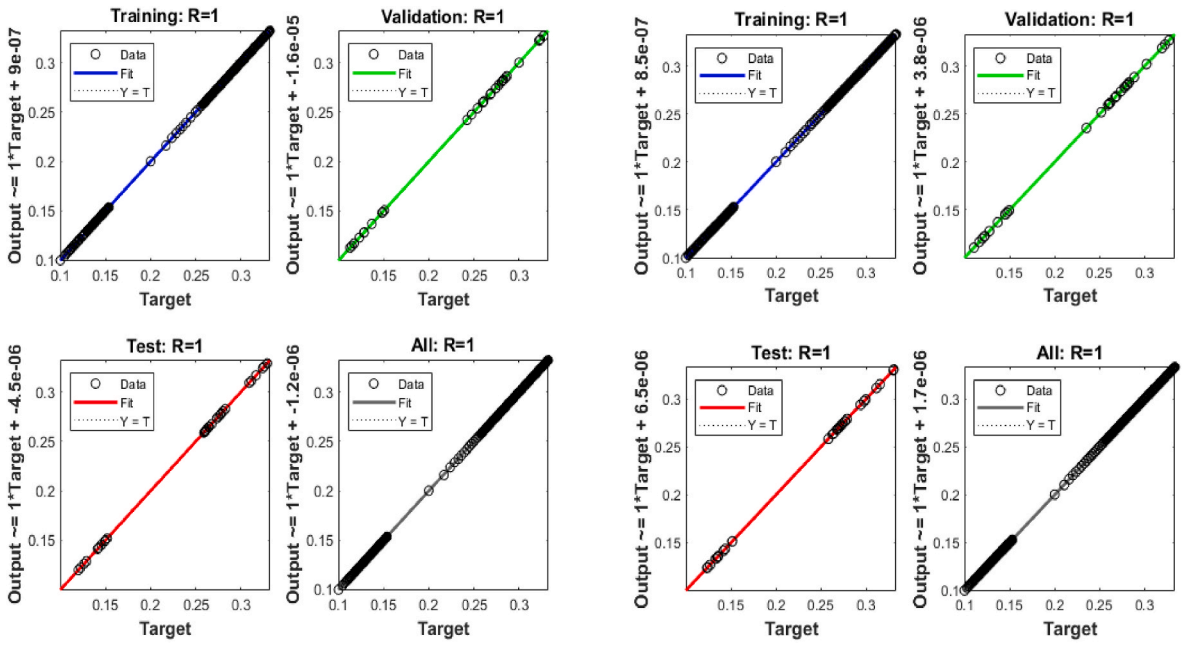

(a) Regression (1) (b) Regression (2)

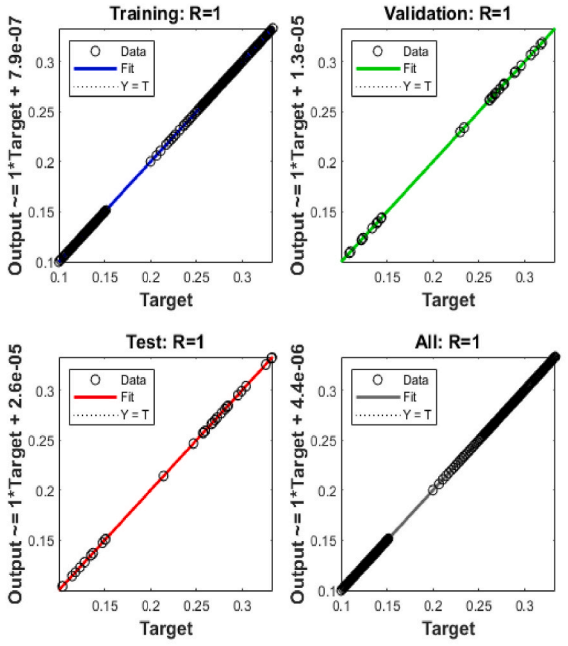

(c) Regression (3)

Fig. 5. Regression values for the FMBDS.

Table 3
MSE performances using the ANN-SCGPs for FMBDS.

Case	MSE			Performance	Gradient	Mu	Epoch	Time
	[Training]	[Verification]	[Testing]					
I	5.924×10^{-09}	2.346×10^{-09}	1.20×10^{-09}	5.92×10^{-09}	8.64×10^{-08}	1×10^{-10}	38	2 Sec
2	1.737×10^{-09}	2.456×10^{-10}	2.90×10^{-10}	1.74×10^{-09}	9.77×10^{-08}	1×10^{-10}	63	3 Sec
3	9.799×10^{-10}	4.595×10^{-10}	3.29×10^{-09}	9.80×10^{-10}	9.93×10^{-08}	1×10^{-10}	40	2 Sec

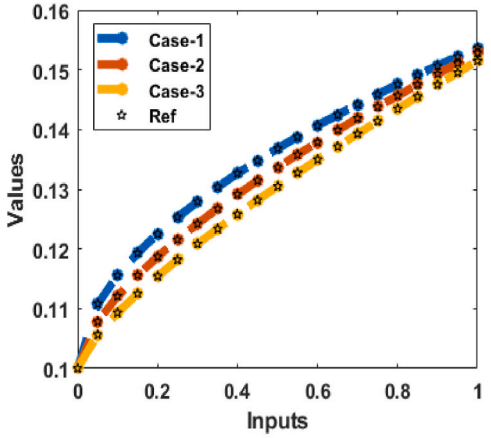

(a) Results: $C(\theta)$

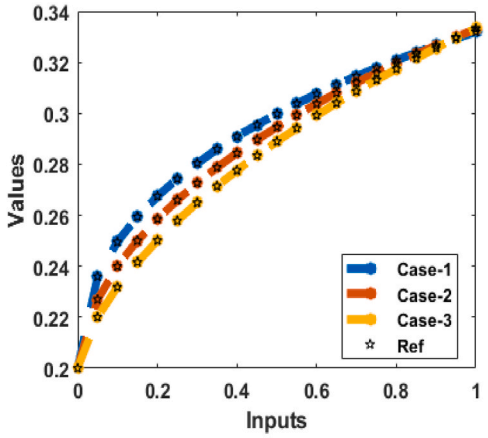

(b) Results: $B(\theta)$

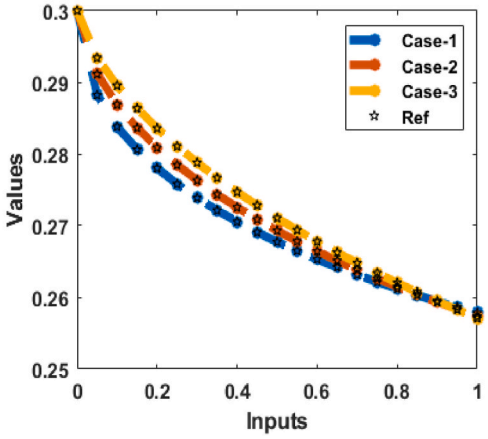

(c) Results $T(\theta)$

Fig. 6. Result comparison using the ANN-SCGPs for the FMBDS.

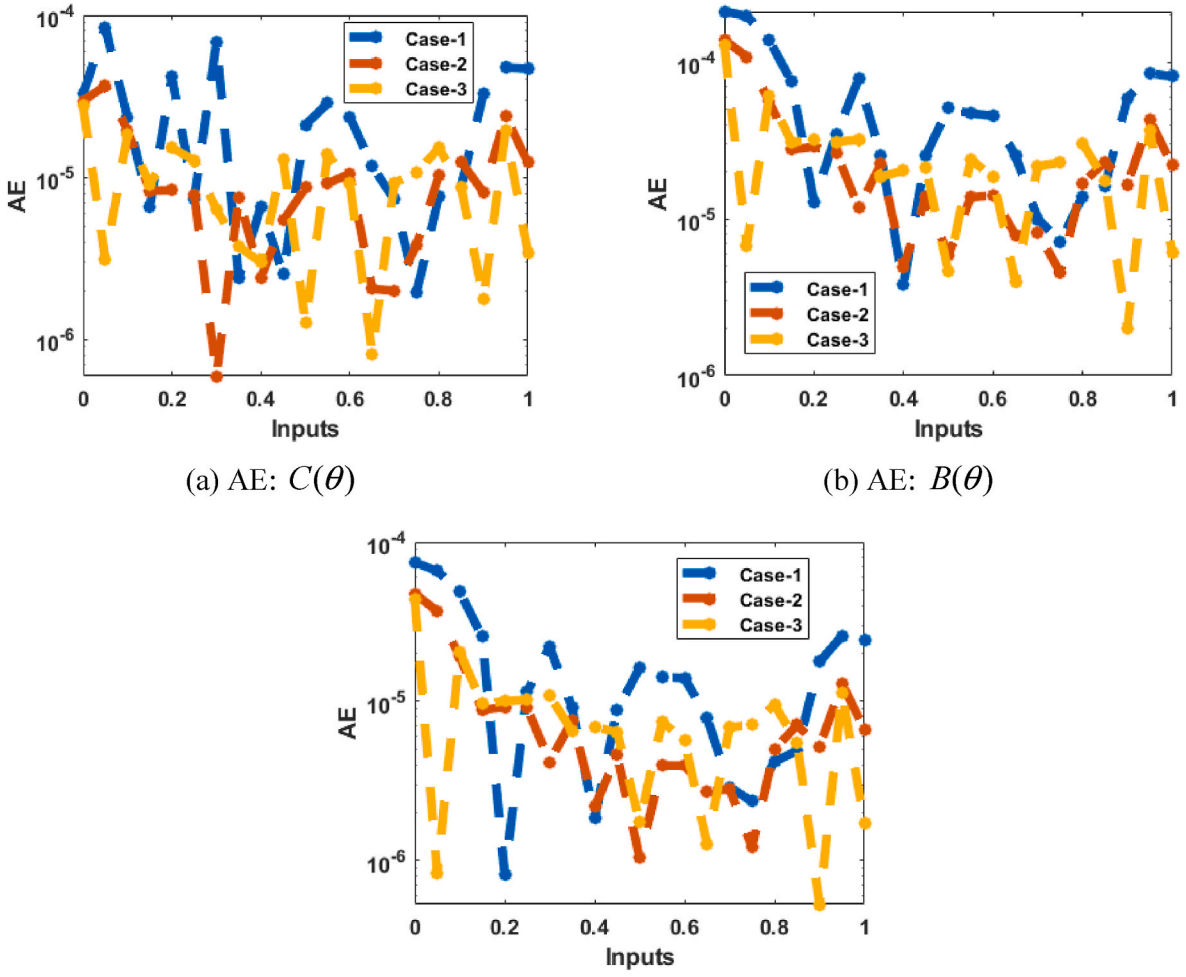

Fig. 7. Performances of the AE using the ANN-SCGPs for the FMBDS.

- The exactness of the ANN-SCGPs is performed by using the comparison performances of the proposed and reference solutions.
- The fractional order derivatives have been provided for 0.5, 0.6 and 0.7 and it is noticed that the results based on 0.7 are more accurate as compared to other two derivative values.
- The consistency, validity, precision, and capability of the ANN-SCGPs can be judged through analysis of the STs values, regression actions, correlation behaviors, EHs, and MSE data.

In future, the ANNs-SCGPs procedure is presented to solve the nonlinear differential mathematical models [45–53].

Declaration of competing interest

The authors declare that they have no known competing financial interests or personal relationships that could have appeared to influence the work reported in this paper.

Acknowledgements

W. Cholamjiak would like to thank National Research Council of Thailand (NRCT) and Thailand Science Research and Innovation, the University of Phayao (FF66-UoE).

References

[1] Parfitt AM. Osteonal and hemi-osteonal remodeling: the spatial and temporal framework for signal traffic in adult human bone. J Cell Biochem 1994;55(3):273–86.
[2] Martin MJ, Buckland-Wright JC. Sensitivity analysis of a novel mathematical model identifies factors determining bone resorption rates. Bone 2004;35(4):918–28.
[3] Lekszycki T. Functional adaptation of bone as an optimal control problem. J Theor Appl Mech 2005;43(3):555–74.
[4] Martínez G, Aznar JMG, Doblaré M, Cerrolaza M. External bone remodeling through boundary elements and damage mechanics. Math Comput Simulat 2006;73(1–4):183–99.
[5] Maldonado S, Findeisen R, Allgower F. Describing force-induced bone growth and adaptation by a mathematical model. J Musculoskelet Neuronal Interact 2008;8(1):15–7.
[6] Tezuka KI, Wada Y, Takahashi A, Kikuchi M. Computer-simulated bone architecture in a simple bone-remodeling model based on a reaction-diffusion system. J Bone Miner Metabol 2005;23(1):1–7.
[7] Lemaire V, Tobin FL, Greller LD, Cho CR, Suva LJ. Modeling the interactions between osteoblast and osteoclast activities in bone remodeling. J Theor Biol 2004;229(3):293–309.
[8] Moroz A, Wimpenny DI. Allosteric control model of bone remodelling containing periodical modes. Biophys Chem 2007;127(3):194–212.
[9] Pivonka P, Zimak J, Smith DW, Gardiner BS, Dunstan CR, Sims NA, Martin TJ, Mundy GR. Model structure and control of bone remodeling: a theoretical study. Bone 2008;43(2):249–63.
[10] Restrepo JM, Choksi R, Hyman JM, Jiang Y. Improving the damage accumulation in a biomechanical bone remodelling model. Comput Methods Biomech Biomed Eng 2009;12(3):341–52.
[11] Ryser MD, Nigam N, Komarova SV. Mathematical modeling of spatio-temporal dynamics of a single bone multicellular unit. J Bone Miner Res 2009;24(5):860–70.
[12] Mundy GR. Myeloma bone disease. Eur J Cancer 1998;34(2):246–51.

[13] Mundy GR, Raisz LG, Cooper RA, Schechter GP, Salmon SE. Evidence for the secretion of an osteoclast stimulating factor in myeloma. N Engl J Med 1974;291 (20):1041–6.
[14] Bataille R, Chappard D, Marcelli C, Dessauw P, Baldet P, Sany J, Alexandre C. Recruitment of new osteoblasts and osteoclasts is the earliest critical event in the pathogenesis of human multiple myeloma. J Clin Invest 1991;88(1):62–6.
[15] Valentin-Opran A, Charhon SA, Meunier PJ, Edouard CM, Arlot ME. Quantitative histology of myeloma-induced bone changes. Br J Haematol 1982;52(4):601–10.
[16] Taube T, Beneton MN, McCloskey EV, Rogers S, Greaves M, Kanis JA. Abnormal bone remodelling in patients with myelomatosis and normal biochemical indices of bone resorption. Eur J Haematol 1992;49(4):192–8.
[17] Evans CE, Galasko CS, Ward C. Does myeloma secrete an osteoblast inhibiting factor? J Bone Jt Surg Br Vol 1989;71(2):288–90.
[18] Bataille R, Delmas PD, Chappard D, Sany J. Abnormal serum bone Gla protein levels in multiple myeloma: crucial role of bone formation and prognostic implications. Cancer 1990;66(1):167–72.
[19] Abildgaard N, Rungby J, Glerup H, Brixen K, Kassem M, Brincker H, Heickendorff L, Eriksen EF, Nielsen JL. Long-term oral pamidronate treatment inhibits osteoclastic bone resorption and bone turnover without affecting osteoblastic function in multiple myeloma. Eur J Haematol 1998;61(2):128–34.
[20] Woitge HW, Horn E, Keck AV, Auler B, Seibel MJ, Pecherstorfer M. Biochemical markers of bone formation in patients with plasma cell dyscrasias and benign osteoporosis. Clin Chem 2001;47(4):686–93.
[21] Komarova SV, Smith RJ, Dixon SJ, Sims SM, Wahl LM. Mathematical model predicts a critical role for osteoclast autocrine regulation in the control of bone remodeling. Bone 2003;33(2):206–15.
[22] Akchurin T, Aissiou T, Kemeny N, Prosk E, Nigam N, Komarova SV. Complex dynamics of osteoclast formation and death in long-term cultures. PLoS One 2008; 3(5):e2104.
[23] Komarova SV. Mathematical model of paracrine interactions between osteoclasts and osteoblasts predicts anabolic action of parathyroid hormone on bone. Endocrinology 2005;146(8):3589–95.
[24] Komarova SV. Bone remodeling in health and disease: lessons from mathematical modeling. Ann N Y Acad Sci 2006;1068(1):557–9.
[25] Sabir Z. Stochastic numerical investigations for nonlinear three-species food chain system. Int J Biomath (IJB) 2022;15(4):2250005.
[26] Sabir Z, Ali MR, Sadat R. Gudermannian neural networks using the optimization procedures of genetic algorithm and active set approach for the three-species food chain nonlinear model. J Ambient Intell Hum Comput 2022:1–10.
[27] Souayeh B, Sabir Z, Umar M, Alam MW. Supervised neural network procedures for the novel fractional food supply model. Fractal Fract. 2022;6(6):333.
[28] Sabir Z, Amin F, Pohl D, Guirao JL. Intelligence computing approach for solving second order system of Emden-Fowler model. J Intell Fuzzy Syst 2020;38(6): 7391–406.
[29] Sabir Z. Neuron analysis through the swarming procedures for the singular two-point boundary value problems arising in the theory of thermal explosion. The Eur. Phys. J. Plus 2022;137(5):638.
[30] Sabir Z, Wahab HA. Evolutionary heuristic with Gudermannian neural networks for the nonlinear singular models of third kind. Phys Scripta 2021;96(12):125261.
[31] Umar M, Amin F, Wahab HA, Baleanu D. Unsupervised constrained neural network modeling of boundary value corneal model for eye surgery. Appl Soft Comput 2019;85:105826.
[32] Wang B, Gomez-Aguilar JF, Sabir Z, Raja MAZ, Xia WF, Jahanshahi H, Alassafi MO, Alsaadi FE. Numerical computing to solve the nonlinear corneal system of eye surgery using the capability of Morlet wavelet artificial neural networks. Fractals. 2022, 2240147.
[33] Sabir Z, Raja MAZ, Alnahdi AS, Jeelani MB, Abdelkawy MA. Numerical investigations of the nonlinear smoke model using the Gudermannian neural networks. Math Biosci Eng 2022;19(1):351–70.
[34] Saeed T, Sabir Z, Alhodaly MS, Alsulami HH, Sánchez YG. An advanced heuristic approach for a nonlinear mathematical based medical smoking model. Results Phys 2022;32:105137.
[35] Mukdasai K, Sabir Z, Raja MAZ, Sadat R, Ali MR, Singkibud P. A numerical simulation of the fractional order Leptospirosis model using the supervise neural network. Alex Eng J 2022;61(12):12431–41.
[36] Botmart T, Sabir Z, Raja MAZ, Ali MR, Sadat R, Aly AA, Saad A. A hybrid swarming computing approach to solve the biological nonlinear Leptospirosis system. Biomed Signal Process Control 2022;77:103789.
[37] Guerrero Sánchez Y, Sabir Z, Günerhan H, Baskonus HM. Analytical and approximate solutions of a novel nervous stomach mathematical model. Discrete Dynam Nat. Soc. 2020.
[38] Sabir Z, Raja MAZ, Mahmoud SR, Balubaid M, Algarni A, Alghtani AH, Aly AA, Le DN. A novel design of morlet wavelet to solve the dynamics of nervous stomach nonlinear model. Int J Comput Intell Syst 2022;15(1):1–15.
[39] Ayati BP, Edwards CM, Webb GF, Wikswo JP. A mathematical model of bone remodeling dynamics for normal bone cell populations and myeloma bone disease. Biol Direct 2010;5(1):1–17.
[40] Elsonbaty AMR, Sabir Z, Ramaswamy R, Adel W. Dynamical analysis of a novel discrete fractional SITRS model for COVID-19. Fractals 2021;29(8):2140035.
[41] Botmart T, Sabir Z, Raja MAZ, Weera W, Sadat R, Ali MR. A numerical study of the fractional order dynamical nonlinear susceptible infected and quarantine differential model using the stochastic numerical approach. Fractal Fract. 2022;6 (3):139.
[42] Souayeh B, Sabir Z, Hdhiri N, Al-Kouz W, Alam MW, Alsheddi T. A stochastic bayesian regularization approach for the fractional food chain supply system with allee effects. Fractal Fract. 2022;6(10):553.
[43] Sabir Z, Munawar M, Abdelkawy MA, Raja MAZ, Ünlü C, Jeelani MB, Alnahdi AS. Numerical investigations of the fractional-order mathematical model underlying immune-chemotherapeutic treatment for breast cancer using the neural networks. Fractal Fract. 2022;6(4):184.
[44] Akkilic AN, Sabir Z, Raja MAZ, Bulut H. Numerical treatment on the new fractional-order SIDARTHE COVID-19 pandemic differential model via neural networks. The Eur. Phys. J. Plus 2022;137(3):1–14.
[45] Vajravelu K, Sreenadh S, Saravana R. Influence of velocity slip and temperature jump conditions on the peristaltic flow of a Jeffrey fluid in contact with a Newtonian fluid. Appl. Math. Nonlinear Sci. 2017;2(2):429–42.
[46] Selvi MSM, Rajendran L. Application of modified wavelet and homotopy perturbation methods to nonlinear oscillation problems. Appl. Math. Nonlinear Sci. 2019;4(2):351–64.
[47] Sabir Z, Botmart T, Raja MAZ, Weera W. An advanced computing scheme for the numerical investigations of an infection-based fractional-order nonlinear prey-predator system. PLoS One 2022;17(3):e0265064.
[48] Gürbüz, M M, Yıldız Ç. Some new inequalities for convex functions via Riemann-Liouville fractional integrals. Appl. Math. Nonlinear Sci. 2021;6(1):537–44.
[49] Sabir Z, Raja MAZ, Nguyen TG, Fathurrochman I, Sadat R, et al. Applications of neural networks for the novel designed of nonlinear fractional seventh order singular system. Eur Phys J Spec Top 2022:1–15.
[50] Akdemir AO, Deniz E, Yüksel E. On some integral inequalities via conformable fractional integrals. Appl. Math. Nonlinear Sci. 2021;6(1):489–98.
[51] İlhan E, Kıymaz İO. A generalization of truncated M-fractional derivative and applications to fractional differential equations. Appl. Math. Nonlinear Sci. 2020;5 (1):171–88.
[52] Yokuş A, Gülbahar S. Numerical solutions with linearization techniques of the fractional Harry Dym equation. Appl. Math. Nonlinear Sci. 2019;4(1):35–42.
[53] Gençoğlu MT, Agarwal P. Use of quantum differential equations in sonic processes. Appl. Math. Nonlinear Sci. 2021;6(1):21–8.